Downslope Wind Verification of the National Blend of Models v4.0 Across the Northern Front Range of Colorado During the 2020/2021 Cool Season

MCKENZIE L. LARSON
Department of Atmospheric and Oceanic Sciences, University of Colorado Boulder, Boulder, Colorado

ANDREW C. WINTERS
Department of Atmospheric and Oceanic Sciences, University of Colorado Boulder, Boulder, Colorado

PAUL T. SCHLATTER
National Weather Service, Boulder, Colorado

ABSTRACT

Downslope windstorms are common leeward of the Rocky Mountains across the High Plains of Colorado during October through March and can cause property damage and travel disruptions. This region is renowned for two primary types of strong downslope winds: (1) chinooks that feature warm, dry winds and are often associated with the development of mountain waves, and (2) boras that are colder and often associated with the passage of a mid- and upper-level trough. The National Blend of Models (NBM) is regularly utilized by forecasters at the National Weather Service Forecast Office (WFO) in Boulder and is one tool used by the WFO to forecast downslope windstorms. No study, however, has quantified the performance of the NBM during downslope windstorms along the Colorado Front Range.

In this exploratory study, downslope windstorms from October 2020 through May 2021 were identified using ten observation sites along the Colorado Front Range. Windstorms were subsequently analyzed to quantify forecast statistics of wind speeds and gusts during windstorms to provide a better understanding of NBM v4.0 performance. On average, we found that the overall maximum magnitudes of wind speeds and gusts are on average 38% and 35% too low in the NBM output, respectively, when averaged across 24 to 72-h lead times. Weather and Research Forecasting (WRF) model simulations of varying vertical resolution were also completed to determine if WRF, a constituent model of the NBM, could provide a robust representation of select downslope windstorms across the Colorado Front Range.

---

1. Introduction

Winds directed down a slope, such as a mountain range, are referred to as "downslope winds" and lead to warming and drying at the Earth's surface leeward of the slope (Glossary of Meteorology 2012). Downslope winds not only affect the local climate of a region but also cause numerous societal impacts that affect day-to-day life, including property damage and travel disruptions. The Colorado Front Range is located in the easternmost section of the Rocky Mountains and is renowned for its frequent downslope windstorms, characterized by

periods of exceptionally strong and violent downslope winds. The mountains of the Colorado Front Range are oriented perpendicular, or nearly perpendicular, to the prevailing wind direction within the middle and upper troposphere, which provides an environment conducive to frequent downslope windstorms.

On 30 December 2021, the Marshall Fire started in conjunction with an intense downslope windstorm that occurred from the mid-morning through the late-afternoon/evening. After a booming growing season during Summer 2021, exceptional drought conditions compounded by a very dry fall led to ideal conditions

Corresponding author address: McKenzie Larson, 311 UCB, Boulder, CO 80309
E-mail: mckenzie.larson@colorado.edu

for rapid fire growth into the towns of Louisville and Superior, Colorado. As a result of the fire, 1084 houses were destroyed (United States Department of Commerce 2022) and two lives were lost. In an early climatology of downslope windstorms, Whiteman and Whiteman (1974) note that fires are not uncommon in conjunction with downslope winds in Boulder, as 57 out of the 151 windstorms in their study had fires reported with them due to downed power lines, failure to properly extinguish campfires, windblown ash, and other sources. Long-range operational model forecasts prior to the Marshall Fire did not capture the initial magnitude and timing of the windstorm well due to their inability to correctly model the synoptic-scale environment, providing limited warning for the strength and timing of this windstorm (Fovell et al. 2022). Given the relationship between fire ignitions and downslope windstorms, improved forecasts for downslope windstorms would also benefit fire weather prediction along the Colorado Front Range, further emphasizing the importance of researching these unique winds across the region.

Downslope windstorm studies along the Colorado Front Range date back to the 1950s. In particular, Ives (1950) noted that downslope windstorms along the Colorado Front Range have a considerable effect on local climate conditions. For example, average winter (DJF) temperatures are warmer in areas adjacent to the Foothills when compared to other Front Range cities, with downslope winds likely playing a role in facilitating these warmer climatological temperatures (National Weather Service 2022). As previously mentioned, downslope windstorms have profound societal impacts and can feature wind speeds >62.6 m s^{-1} (140 mph) (as measured in Boulder, Colorado), which far exceeds the threshold for hurricane force winds (33.1 m s^{-1} or 74 mph) (National Oceanic and Atmospheric Administration 2022). Brinkmann (1974) completed a detailed study of downslope windstorms in Boulder, Colorado, and the most recent climatology for downslope windstorms in Boulder, Colorado, was published by Whiteman and Whiteman (1974) nearly fifty years ago. Whiteman and Whiteman (1974) found that strong downslope winds leeward of the Rocky Mountains generally occur from Colorado Springs, Colorado, to Cheyenne, Wyoming, with the most damaging winds often occurring in or near Boulder. Temporally, these downslope windstorms occur most frequently in January, followed by November and December, respectively. These windstorms also exhibit

a diurnal frequency distribution, in that they most commonly occur overnight prior to sunrise. Maximum gust speeds, however, often occur during the early afternoon and in the evening during a windstorm. The strongest winds associated with downslope windstorms can last from <1 h to as long as 24 h, with an average windstorm duration of 8.1 h. While these windstorms often exhibit consistently strong winds throughout their durations, the longer storms (up to 24 h) frequently feature pauses between distinct periods of high wind gusts.

In this study, two types of downslope winds are considered: chinooks and boras. Also known as a foehn wind, a chinook is a warm, dry wind that descends on the leeward side of the Rocky Mountains (Brinkmann 1971). There are two mechanisms that can lead to a chinook. These so-called "snow eaters" are produced when cold air becomes dammed on the windward side of a mountain ridge, allowing fast air aloft to descend leeward of the mountain. Chinooks are also formed by orographic forcing when air ascends the windward side of the orography. Moisture subsequently condenses and precipitates out near mountaintop as it rises. From there, the air warms dry adiabatically as it descends on the leeward side of the mountain. This sequence allows the air on the leeward side of the mountain to be warmer than air on the windward side. In contrast, boras are associated with the passage of a mid- and upper-tropospheric trough. These winds are post-cold frontal and occur when cold air masses upstream are deeper than the ridge height of local orography, which allows cold air to channel down the leeward side of the mountain (Durran 1990; Stull 2017). A temperature inversion at 600 hPa and strong wind shear above 600 hPa are typically conducive to the development of a bora. Both chinooks and boras can cause severe wind damage along the Colorado Front Range, so it is imperative that numerical weather prediction models generate accurate and timely forecast guidance in advance of these windstorms.

The complex topography of the northern Colorado Front Range contributes to considerable complexity and difficulty when forecasting downslope windstorms. In particular, numerical weather prediction models often experience difficulty resolving mesoscale or microscale processes (e.g., turbulent mixing, convection, small-scale waves) that occur in regions characterized by complex topography due to their varied vertical and horizontal grid spacing. In many cases, these physical processes cannot be explicitly resolved in operational

models and need to be parameterized. The coarser and long-range forecast models often used by operational forecasters have horizontal resolutions of many kilometers (e.g., 28 km for the Global Forecast System [National Centers for Environmental Information 2020], 32 km/12 km/3 km for the North American Model [NCEP Central Operations 2023]), while the turbulence-resolving models that would better represent downslope windstorms are computationally expensive and not suitable for operational use, especially at long forecast lead times (Goger et al. 2016). Other limitations include the varied temporal resolution of surface observation sites near the Colorado Front Range, sparse vertical profiles of the atmosphere via radiosondes that are limited to twice per day (0000 UTC and 1200 UTC), and the brief forecast lead times associated with high-resolution, mesoscale model forecasts.

Previous studies investigating the predictability of downslope windstorms utilized multi-nested weather simulations and statistical analyses to characterize downslope winds in other geographical regions, such as the Wasatch winds in Utah (Lawson and Horel 2015), Medicine Bow Mountain winds in Wyoming (Pokharel et al. 2017), and Santa Ana and Sundowner winds in California (Cao and Fovell 2016, 2018; Duine et al. 2019). These studies have emphasized the importance of local geography, the character of the synoptic-scale flow pattern, and the vertical atmospheric structure in producing accurate simulations of these winds. In particular, Lawson and Horel (2015) highlighted the importance of the local topography for driving Wasatch winds in Utah, because the Uinta Mountains serve to block and facilitate the northeasterly flow necessary for their development. Furthermore, Pokharel et al. (2017) explained that upstream conditions as well as a self-induced critical level (i.e., where the wind stops or reverses direction in the vertical) are conducive for the formation and persistence of downslope winds in the Medicine Bow Mountains. Cao and Fovell (2016, 2018) were some of the first to identify the importance of roughness length in simulating downslope windstorms from their studies of Santa Ana winds in San Diego County. The authors found the Santa Ana winds are especially sensitive to the land surface models that establish the surface roughness values used within the WRF (Skamarock et al. 2008) model simulations. Additionally, Duine et al. (2019) discussed how the inclusion of higher roughness length values in land surface models can lead to adequate predictions of downslope windstorms. Prior work also emphasized

the importance of the local synoptic-scale environment for establishing a conducive setup for downslope windstorms (Lawson and Horel 2015). Namely, the synoptic-scale flow pattern must provide cross-barrier flow over the local orographic feature (in this study, the Colorado Front Range). Along with utilizing numerical weather prediction models, previous studies have implemented statistical models to forecast downslope winds. For example, Mercer et al. (2008) statistically modeled downslope winds in Boulder, Colorado, and found an underestimation bias for wind speeds and gusts. In summary, although substantial research has been conducted on downslope winds, operational numerical weather prediction models and forecasters continue to face difficulties forecasting the intensity and timing of these impactful windstorms.

The purpose of this study is (1) to identify current biases and errors of wind speeds, gusts, and timing during downslope windstorms across the northern Colorado Front Range within a current state-of-the-art numerical weather prediction tool used operationally and (2) to use this information to improve wind forecasts and warnings for these high-impact windstorms. It is hypothesized that forecasts underestimate the magnitude of wind speeds and gusts for all observational sites along the Colorado Front Range due to the strong—and sometimes extreme—nature of these downslope winds and due to the difficulty in resolving mesoscale and microscale processes that generate downslope winds in numerical weather prediction models.

The National Blend of Models (NBM)—a statistically post-processed blend of multiple numerical weather prediction models used in forecast operations—has become the starting point for much of the National Weather Service's (NWS) gridded forecast information across the United States. The motivation behind the NBM was to combine NWS and non-NWS model output in an optimal manner to provide a reliable initial forecast, so that forecasters can spend more time utilizing their expertise on other aspects of the forecast and decision support (United States Department of Commerce 2023). Specifically, the NBM represents the starting point for gridded 36 h to 7-day forecasts issued by the Boulder NWS WFO. Consequently, it is important to understand how well the NBM forecasts high-impact weather events, including downslope windstorms along the Colorado Front Range. In this exploratory study, we completed a verification of NBM v4.0 forecasts of downslope windstorms during the 2020/2021 cool season along the Colorado Front Range

in order to quantify downslope wind biases in the NBM and to provide a baseline against which to evaluate future versions of the NBM. Our study also combines this statistical verification of NBM forecasts with Weather Research and Forecasting (WRF) model simulations to examine how changing model parameters alters the character of a windstorm that was poorly forecasted by the NBM.

The remainder of this paper is structured as follows. Section 2 introduces our data and methods, including an in-depth description of the NBM and the statistical verification methods used to evaluate the performance of the NBM. Section 3 introduces the NBM verification results and the windstorm case study, section 4 discusses our results and their implications in the context of previous literature, and section 5 briefly summarizes the main results of the study.

2. Data and methods

a. Observational sites

To identify downslope windstorms along the Colorado Front Range, ten observational sites were used to obtain surface observation data (Fig. 1). These sites include Buckeye (BEYC2), Northern Colorado Regional Airport (KFNL), Colorado Plains Regional Airport (KAKO), Boulder Municipal Airport (KBDU), Sugarloaf (BTAC2), Broomfield/Jefferson County (KBJC), Denver International Airport (KDEN), Pickle Gulch (PKLC2), Berthoud Pass (K0CO), and Lookout Mountain (LOOC2). Data were obtained from the MESOWEST database (Horel et al. 2002a, b) and downloaded for every month during the 2020-2021 downslope windstorm season (October to May). Each data file includes temperature, dewpoint, relative humidity, wind speed, gust speed, wind direction, pressure, and weather codes. The temporal resolution of the observational dataset ranges from five minutes to one hour depending on the site. Automated Surface Observing System (ASOS) and Automated Weather Observing System (AWOS) stations often had a finer temporal resolution than the Interagency Remote Automatic Weather Stations (RAWS). In Fig. 1, the ASOS, AWOS, and RAWS stations are denoted with stars, squares, and circles, respectively.

Known to local forecasters as a weather station that captures most downslope windstorms along the Colorado Front Range, the CO-93/72 site (Colorado Department of Transportation observation station
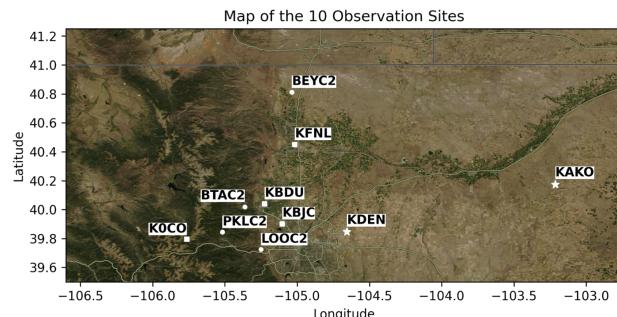

Figure 1. Map of the 10 observational sites examined in this study. Sites denoted with stars indicate Automated Surface Observing System (ASOS) stations. Sites denoted with squares indicate Automated Weather Observing System (AWOS) stations. Sites denoted with circles indicate Interagency Remote Automatic Weather Stations (RAWS). *Click image for an external version; this applies to all figures hereafter.*

CO109 located just east of the Front Range and slightly southwest of KBJC) was used to preliminarily identify downslope windstorms. To do so, changes in wind direction, wind speed and gusts, humidity, and temperature were used as a method to isolate potential downslope windstorms. Details about how these variables evolve during downslope windstorms are described in the following paragraph. After isolating potential windstorms between October 2020 and May 2021 at the CO-93/72 site, observational data from the ten sites investigated in this study (Fig. 1) were examined to see if windstorms that impacted sites within more complex terrain (i.e., K0CO, PKLC2, BTAC2, and LOOC2) extended farther east into more populous regions of the northern Colorado Front Range (i.e., KBDU, KDEN, KFNL, etc.). Not all windstorms impacting sites within complex terrain affected locations farther east, demonstrating the occasionally isolated nature of downslope windstorms in this area and their dependence on meteorological factors that enable the development of strong winds leeward of the mountains.

To isolate more intense downslope windstorms during the 2020/2021 Cool Season, wind gusts were required to exceed a threshold of $\geq$13.4 m s^{-1} (30 mph or 26 kt) at a majority of observational sites along the northern Colorado Front Range in order to qualify as a downslope windstorm. Along with strong wind gusts, downslope windstorms are also associated with changes in temperature and wind direction. As noted by forecasters from the NWS WFO in Boulder, downslope windstorms require at least 7.7 to 15.4 m s^{-1} (15 to 30 kt)

cross-barrier flow above the Rocky Mountains within a kilometer of the ridge top (generally between 500 and 600 hPa) with a wind direction between 240º and 330º (southwesterly to northwesterly). For the identification of windstorms in this study, it was generally required that the winds stayed within this wind direction interval. Boras were manually identified based on the presence of strong wind gusts, northwesterly flow, and a sharp decrease in temperatures associated with a frontal passage, whereas chinooks were manually identified by the presence of strong wind gusts, west to northwesterly flow, and an increase in temperatures. Since some observational sites only record one observation per hour, a lenient time period of at least 3 h was used to confirm the presence of a windstorm. Eleven downslope windstorms were identified between October 2020 and May 2021 using the above criteria. The maximum wind speeds and gusts at each site during the windstorms are shown in Tables 1 and 2. In these tables, sites with an observed maximum wind speed and gust that did not meet the 13.4 m s^{-1} (30 mph) gust threshold in association with a downslope windstorm are excluded from the analysis.

b.   National Blend of Models

The National Blend of Models (NBM) is a state-of-the-art statistically post-processed multi-model ensemble that is used twice daily (or more) by forecasters at the NWS. The NBM integrates both NWS and non-NWS numerical weather prediction model data, as well as post-processed model guidance, to create a single deterministic forecast (NOAA Meteorological Development Laboratory 2021). The 42 different model inputs (not including individual ensemble members) included in the NBM v4.0 are derived from five global modeling centers: United States National Centers for Environmental Prediction (NCEP), Canadian Meteorological Centre (CMC), Naval Fleet Numerical Meteorology and Oceanography Center (FNMOC), European Center for Medium Range Weather Forecasts (ECMWF), and the Bureau of Meteorology (BoM) Australia (Craven et al. 2020; NOAA Meteorological Development Laboratory 2023). The NBM features a horizontal resolution of 2.5 km over the Continental United States (CONUS) and outputs forecasts for temperature, precipitation, moisture, wind, winter weather, fire weather, aviation, and marine elements.

To compare the observational data from the 10 observational sites to NBM v4.0 forecasts during the

11 downslope windstorms, NBM forecast data were downloaded from NOAA's NBM 1D Viewer (National Oceanic and Atmospheric Administration 2021) that extracts data from the closest NBM grid cell to the observational sites. This study subsequently focuses on a verification of NBM forecasts initialized 24 h, 48 h, and 72 h prior to downslope windstorms. Consequently, forecasts were downloaded from the NBM at these three lead times for the individual sites and each windstorm. The NBM forecasts from the 1D Viewer begin at 0100 UTC, 0700 UTC, 1300 UTC, and 1900 UTC for each day. After identifying the time of the peak gust at each observation site, NBM output was downloaded at the last model start time prior to, or that coincided with, the earliest peak gust observed across all sites. From there, observational data and forecast data were matched, accounting for differences in the temporal resolution of the datasets (i.e., NBM forecasts are output once every hour at lead times <24 h and every three hours at lead times >24 h). After matching up the observational data with the NBM forecasts for each site, various analysis methods were completed to perform a verification of the NBM during these windstorms.

For the NBM verification, three different analyses were conducted for each windstorm: a comparison of the NBM forecasts using the (1) lead hour, (2) hourly maximum, and (3) overall maximum wind speed and gusts from each observational site. The lead hour verification involves selecting the wind speed and gust observations that are closest to the top of the hour and comparing those values to the NBM output. The hourly maximum wind speed verification is similar to the lead hour verification, but instead of selecting only the observation at the top of the hour, all of the wind speed and gust observations during the next hour were considered. Finally, the overall maximum wind speed verification considers wind speed and gust observations throughout the windstorm. The purpose of using a longer time period for this final verification method was to ignore model timing errors and to examine how the magnitudes of NBM peak wind speeds and gusts compare with observed peak wind speeds and gusts during a windstorm.

c.   Modeled wind adjustment

Since the anemometer heights vary between the observational sites (10 m at ASOS stations, 9.1 m at AWOS stations, and 6.1 m at RAWS stations), 10 m modeled wind speeds and gusts were adjusted to match

Table 1. Maximum wind speeds at observational sites during each windstorm. The lack of a wind observation indicates a windstorm did not affect the observational site.

Date	KBDU	KBJC	KFNL	K0CO	KDEN	KAKO	BTAC2	PKLC2	LOOC2	BEYC2
10/11/2020	42 kt	48 kt	30 kt		36 kt	38 kt	14 kt	13 kt	21 kt	53 kt
12/16/2020	22 kt	27 kt		44 kt			12 kt	15 kt	12 kt	26 kt
12/20/2020		39 kt		47 kt	21 kt	16 kt	14 kt	23 kt	17 kt	28 kt
12/22/2020	33 kt	35 kt	24 kt	33 kt	37 kt	42 kt	17 kt	20 kt	20 kt	30 kt
1/2/2021	28 kt	21 kt		43 kt				17 kt	11 kt	36 kt
1/20/2021		40 kt		43 kt	24 kt			19 kt	13 kt	20 kt
2/7/2021	21 kt	41 kt	25 kt		33 kt	28 kt	10 kt	14 kt	16 kt	31 kt
2/23/2021	22 kt	29 kt	22 kt	54 kt	29 kt	36 kt	11 kt	13 kt	10 kt	15 kt
3/29/2021	28 kt	30 kt	30 kt	53 kt	25 kt		12 kt	14 kt	14 kt	35 kt
4/7/2021	24 kt	16 kt	24 kt	35 kt	20 kt	29 kt	9 kt	16 kt	9 kt	25 kt
5/8/2021	21 kt	27 kt	28 kt	28 kt		28 kt	5 kt	12 kt	12 kt	24 kt

Table 2. Maximum wind gusts at observational sites during each windstorm. The lack of a wind observation indicates a windstorm did not affect the observational site.

Date	KBDU	KBJC	KFNL	K0CO	KDEN	KAKO	BTAC2	PKLC2	LOOC2	BEYC2
10/11/2020	50 kt	58 kt	38 kt		48 kt	59 kt	30 kt	30 kt	37 kt	71 kt
12/16/2020	36 kt	39 kt		52 kt			26 kt	55 kt	28 kt	38 kt
12/20/2020		48 kt		61 kt	31 kt	29 kt	31 kt	56 kt	36 kt	43 kt
12/22/2020	53 kt	50 kt	45 kt	55 kt	52 kt	59 kt	52 kt	49 kt	47 kt	61 kt
1/2/2021	35 kt	31 kt		48 kt				42 kt	25 kt	50 kt
1/20/2021		50 kt		52 kt	33 kt			48 kt	35 kt	39 kt
2/7/2021	38 kt	53 kt	34 kt		47 kt	33 kt	25 kt	32 kt	35 kt	47 kt
2/23/2021	31 kt	40 kt	28 kt	73 kt	37 kt	47 kt	26 kt	37 kt	24 kt	39 kt
3/29/2021	43 kt	38 kt	38 kt	64 kt	37 kt		28 kt	37 kt	27 kt	62 kt
4/7/2021	33 kt	26 kt	26 kt	44 kt	29 kt	38 kt	21 kt	42 kt	24 kt	42 kt
5/8/2021	38 kt	43 kt	33 kt	45 kt		38 kt	31 kt	31 kt	25 kt	45 kt

the anemometer height at the observational sites via the power law profile wind adjustment. As shown in Equation 1, a power law wind adjustment calculates the adjusted modeled wind speed and gusts (V_h) by multiplying the modeled 10 m wind speed and gusts by a factor that accounts for differences in anemometer height ($h/10\ m$) and is raised to a power law coefficient (α). Since downslope windstorms can be quite intense and can lead to a well-mixed boundary layer, we allow $\alpha = 1/7$ to represent a neutrally stable environment. This assumption is also made for because we do not have access to observed atmospheric vertical profiles at the AWOS and RAWS sites to calculate the atmospheric stability above each of these locations.

$$V_h = V_{10}(h/10\ m)^{\alpha} \qquad \text{(Eq. 1)}$$

Here, a power law profile was used to adjust the NBM 10 m winds to station anemometer heights so that the forecasts are directly comparable to the AWOS

9.1 m and RAWS 6.1 m winds speeds and gusts. This equation is commonly used in the wind engineering field because it does not require the knowledge of the surface roughness or friction velocity, which are often not available (Brower 2012, Lundquist 2022).

As with other modeled wind gust output from numerical weather prediction models, the interpretation of the 10 m wind gusts may not necessarily be an exact 1:1 comparison with wind gust observations. However, the purpose of this study is to quantify how the NBM output directly compares with observational data. Consequently, we do not apply any additional wind gust adjustments (i.e., a gust potential) beyond adjusting for various observational anemometer heights.

d. *Statistical verification*

For each individual verification method, the performance of NBM forecasts is evaluated based on the mean absolute errors (MAEs), correlations, and multiplicative

biases (MB) of wind speeds and gusts during each windstorm. As shown in Equation 2, the MAE can be quantified by subtracting the observed wind speed or gust (O_i) from the NBM forecasted value (F_i) during a specific time period and taking the absolute value of this difference. From there, this value is summed across the total number of observations/forecast data points and divided by the total number of observation/forecast data points (n). The MAE characterizes the average error of the NBM during downslope windstorms and can be used to characterize the relationship between model error and peak wind speeds and gusts during downslope windstorms.

$$\text{MAE} = \frac{\sum_{i=1}^{n} |F_i - O_i|}{n} \qquad \text{(Eq. 2)}$$

To investigate the aforementioned relationship between observed and forecasted peak wind speeds and gusts, correlation tests were performed between the NBM MAE and observed wind data. A positive correlation indicates poor model performance (i.e., greater MAE is present when larger peak gusts occur); the opposite is true with a negative correlation, indicating better model performance (i.e., greater MAE is present when smaller peak gusts occur). The observed peak wind speed and gust data were not normal (Shapiro Test, $p < 0.05$), so Spearman Correlation Tests were used. Another statistic used in this study is the MB, or how the average magnitude of NBM forecasted wind speeds and gusts compares with the average magnitude of the observations. As shown in Equation 3, this bias is quantified by dividing the average NBM forecasted wind speed or gust (F_i) by the average observed wind speed or gust (O_i), respectively. A MB below 1 indicates that the NBM is underestimating the wind speed and/or gust. This bias can subsequently be utilized by forecasters to understand how much the NBM is underestimating or overestimating wind speeds and gusts (separately) during downslope windstorms.

$$\text{MB} = \frac{\frac{1}{n}\sum_{i=1}^{n} F_i}{\frac{1}{n}\sum_{i=1}^{n} O_i} \qquad \text{(Eq. 3)}$$

e.   Timing errors

By utilizing NBM forecast and observational data during the 15 h time period centered on the observed peak wind gust (Fig. 2), timing errors were quantified for all sites during each windstorm. Namely, for each
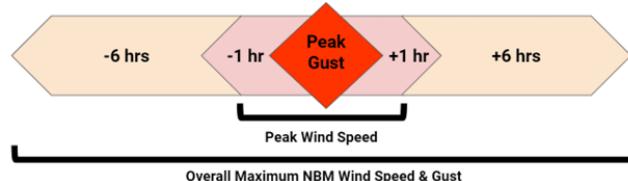

Figure 2. Schematic summarizing the methods used to determine the peak wind speed and gust associated with each windstorm within the NBM forecasts.

site and windstorm, the time of the observed peak gust was identified, and the time of the observed peak wind speed was identified within a time period of ±1 h of the peak gust time. From there, ±6 h were added onto this 3-h time period to create a larger, 15 h time window of NBM forecast data to compare with the observational data. The timing of peak wind speeds and gusts within the 24 h, 48 h, and 72 h NBM forecasts prior to each windstorm were then compared to the timing of the observed peak wind speed and gust at each site. The overall average across all sites during all eleven windstorms was subsequently calculated, as well as individual average timing errors as a function of observational site. This analysis permits an investigation of how accurately the NBM predicts the timing of downslope windstorms.

f.   Weather Research and Forecasting model

The WRF is a numerical weather prediction model that is often utilized for investigating mesoscale and microscale meteorological phenomena. WRF uses a similar dynamical core as other numerical weather prediction models included in the NBM, such as the High-Resolution Rapid Refresh Model (HRRR) and the Rapid Refresh Model (RAP). Two WRF versions, WRF Member Two (WRF MEM2) and the Advanced Research WRF (WRF ARW), are also included in the NBM. Therefore, completing WRF simulations of a particularly notable high-impact downslope windstorm during the 2020/2021 cool season enables further investigation into the predictability of these windstorms and helps provide additional context for the NBM forecast statistics.

To investigate a specific downslope windstorm (22 December 2020) in which the NBM performed poorly, four WRF downslope windstorm simulations with varying vertical resolutions were performed. By increasing the vertical resolution and using a finer horizontal resolution for the model, it was hypothesized that the WRF simulations would be able to effectively

capture the higher wind speeds observed during the 22 December 2020 windstorm. The NBM's finest horizontal resolution is 2.5 km, which may be too large of a grid cell to capture the abrupt change in topography that characterizes the leading edge of the foothills of the Colorado Front Range. Therefore, as shown in Fig. 3, a 9 km domain with two nested domains (3 km and 1 km, respectively) were used to provide a finer horizontal resolution within all four simulations. The use of nested domains, as well as an innermost domain with a horizontal resolution of 1 km, is consistent with previous studies that examine the performance of NWP during downslope windstorms (Lawson and Horel 2015; Pokharel et al. 2017; Duine et al. 2019).

Increasing vertical resolution within the model increases the number of vertical layers, which provides a more effective way of capturing the detailed vertical temperature and wind structure that characterizes downslope windstorms. A simulation with 40 vertical levels (vert40) and 73 vertical levels (vert73) were completed, as well as simulations with 40 user-defined eta levels (vert40_eta) and 73 user-defined eta levels (vert73_eta). Without defining specific eta levels in the model, WRF assigns its own vertical level distribution. By defining specific eta levels, it is possible to have more levels closer to the surface where the downslope windstorms are occurring. The hyperbolic tangent function was used to define the 40 eta levels because this function allows for a smooth vertical transition in positioning the vertical levels in the model. The same vertical levels from Muñoz-Esparza et al. (2018; their Fig. 4b) were used to define the 73 eta levels in this study. For the WRF simulations performed for this study, a maximum vertical thickness of 1000 m and a 50
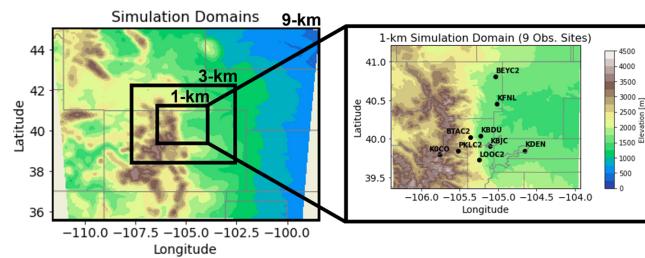

Figure 4. Scatter plots of the mean absolute errors (MAEs) of NBM forecasts compared with observed peak wind speeds and gusts. The first row is the MAE of wind speeds, and the second row is the MAE of wind gusts. The columns identify the errors for various forecast lead times (left-to-right: 24 hr, 48 hr, and 72 hr). The linear fit lines for the wind speeds and gusts (green and blue lines, respectively) show a direct relationship between the NBM MAE and the observations.

m thickness for the bottommost layer were used (WRF defaults). A full summary of the WRF parameterizations and schemes used for each simulation are described in Table 3. These parameterizations and schemes are chosen to be consistent with other recent studies on downslope windstorms (Lawson and Horel 2015; Pokharel et al. 2017; Duine et al. 2019). The model was run from 1200 UTC 22 December 2020 to 1200 UTC 23 December 2020, to allow for approximately 12 h of spin-up time for each simulation. The WRF 10 m wind speeds used in this study were extracted from the closest grid cell to each individual observational site to facilitate direct comparison (Ladwig 2017).

3. Analysis

The forthcoming analysis considers the MAEs, MBs, and timing errors of the NBM during eleven downslope windstorms identified during the 2020/2021 cool season. We then examine a case study of one particularly poorly forecasted windstorm on 22 December 2020.

a. Mean absolute errors

As shown in Fig. 4, there is a direct relationship between the peak observation wind speed and gust to the NBM MAE. This relationship indicates that as the observed peak wind speeds and gusts increase during downslope windstorms, the MAE of model forecasts

Figure 3. WRF domains used to simulate the 22 December 2020 downslope windstorm across the northern Colorado Front Range. The domains consist of one larger, 9 km resolution domain and two nested domains (3 km and 1 km resolutions), shown on the left. The innermost 1 km domain is shown to the right. The black dots represent the 10 observational sites used in this study.
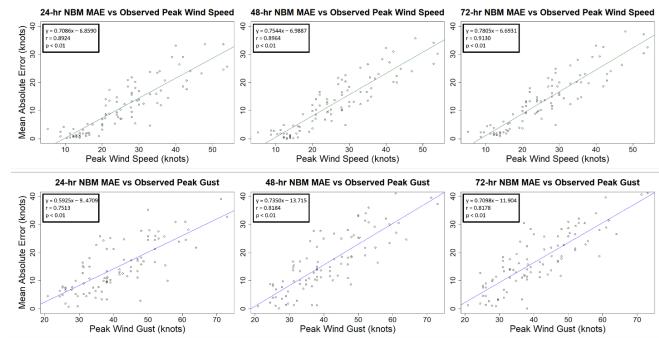
Table 3. Summary of WRF parameterizations used in the low and high vertical resolution simulations performed as part of this study.

	40 Vertical Levels Simulation (vert40)	73 Vertical Levels Simulation (vert73)	40 Eta Vertical Levels Simulation (vert40_eta)	73 Eta Vertical Levels Simulation (vert73_eta)
Vertical levels	40	73	40	73
User-defined eta levels	No	No	Yes	Yes
Microphysics	Thompson (Thompson et al. 2008)			
Cumulus	Kain-Fritsch (Kain 2004) on 9km			
Shortwave/longwave radiation	RRTMG (Iacono et al. 2008)			
Surface layer	Eta similarity (Monin and Obukhov 1954; Janjić 1994, 1996, 2002)			
Land-surface model	NOAH land surface model (Tewari et al. 2004)			
Boundary Layer	MYJ (Janjić 1994)			

also increases. Although it would be convenient to identify a uniform value for the NBM error at each observational site during these windstorms, Fig. 4 shows that a uniform model error cannot be discerned because every downslope windstorm features model errors that vary based on the magnitude of the observed wind speed and gust. Consequently, a more useful statistic for evaluating forecast errors during downslope windstorms is the MB, which is described in the next section.

b.   Multiplicative biases

Figure 5 shows the MBs for each observational site as a function of lead hour, hourly maximum, and overall maximum wind speed and gust. The average MB is calculated based on all downslope windstorms observed at each site. Recalling that a MB below one indicates that the NBM is underestimating the observed wind speeds and/or gusts, Fig. 5 demonstrates that the MB falls below one for the majority of the observational sites. The NBM performs most poorly at the Boulder Municipal Airport (KBDU, blue) and Broomfield/Jefferson County (KBJC, orange) sites. At the Boulder Municipal Airport, the MBs are 0.44, 0.35, and 0.33 for the lead hour, hourly maximum, and overall maximum wind speed, respectively. For wind gusts, the MBs are 0.66, 0.52, and 0.48 for the lead hour, hourly maximum, and overall maximum, respectively. Similarly poor MBs for wind speeds and gusts were observed at the Broomfield/Jefferson County site. It is hypothesized the poor prediction of the wind speeds and gusts by the NBM may be due, in part, to each observation site's proximity to the Colorado Front Range.   The NBM
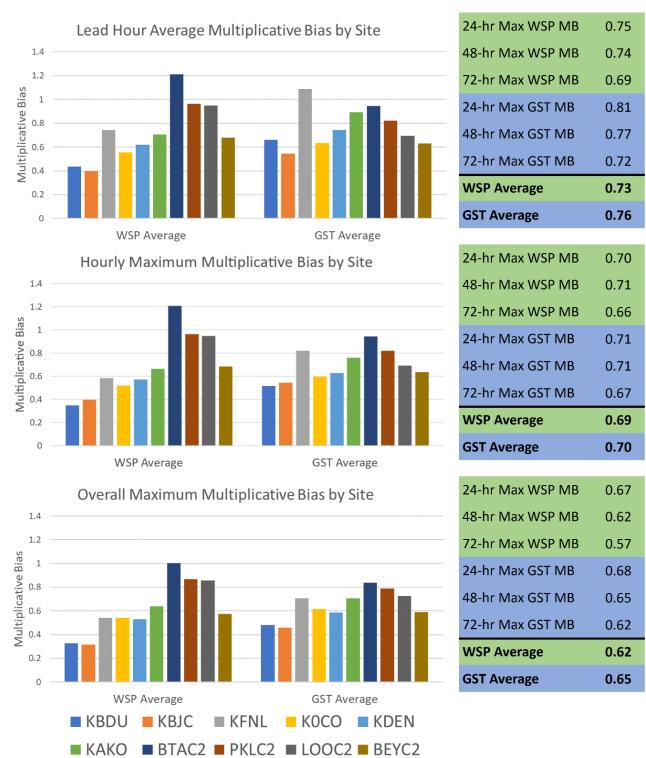

Figure 5. The multiplicative biases of the lead hour (top), hourly maximum (center), and overall maximum (bottom) NBM wind speeds (WSP) and gusts (GST) for each observational site. A multiplicative bias below 1 indicates that the NBM is underestimating the wind speed and/or gust. K0CO was not included in the lead hour verification for the 16 December 2020 windstorm due to missing data, but this site was included in the hourly maximum and overall maximum verification.

performs only as well as its constituents, and only a small subset of the input models have a horizontal resolution of 3 km. Downscaling the input data sources to 2.5 km resolution may not provide a robust and accurate representation of the steep change in topography across this region.

The MBs for Pickle Gulch (PKLC2, dark red) and Lookout Mountain (LOOC2, dark gray) are the closest to one among all of the sites for both forecasted wind speeds and gusts, suggesting better performance by the NBM there. At Pickle Gulch, the MBs are 0.96, 0.96, and 0.87 for the lead hour, hourly maximum, and overall maximum wind speed, respectively. For wind gusts, the MBs are 0.82, 0.82, and 0.79 for the lead hour, hourly maximum, and overall maximum, respectively. Similarly good MBs for wind speeds and gusts were observed at Lookout Mountain and Sugarloaf (BTAC2, dark blue). The average MB for Sugarloaf was often >1, indicating that the NBM frequently overestimated wind speeds and/or gusts at this location during downslope windstorms. The NBM utilizes a statistical correction to inflate wind speeds and gusts in mountainous terrain (UCAR/COMET 2016, 2019). This correction could account for the higher forecasted wind speeds and gusts at observational sites situated within mountainous terrain compared to those sites located across the eastern Plains. Another explanation for the better NBM performance at the mountainous sites could be due to the fact that there was approximately one observation per hour at these sites. Therefore, the same observed wind speed and gust values were used as the lead hour, hourly maximum, and overall maximum values that are considered in this study.

When examining the MBs based on forecast lead time, NBM forecast skill increases when predicting the magnitude of wind speeds and gusts at shorter lead times. This result is demonstrated by the increasing MBs observed in conjunction with shorter forecast lead times for both wind speeds and gusts (green and blue, respectively, in the Fig. 5 tables).

c. Timing errors

Timing errors associated with the NBM during downslope windstorms along the Colorado Front Range improve with decreasing forecast lead time. This is shown via the decrease in the spread of the boxplots for each observational site at shorter forecast lead times in Fig. 6. Nevertheless, the generally large spread of timing errors in Fig. 6 indicates that the NBM poorly
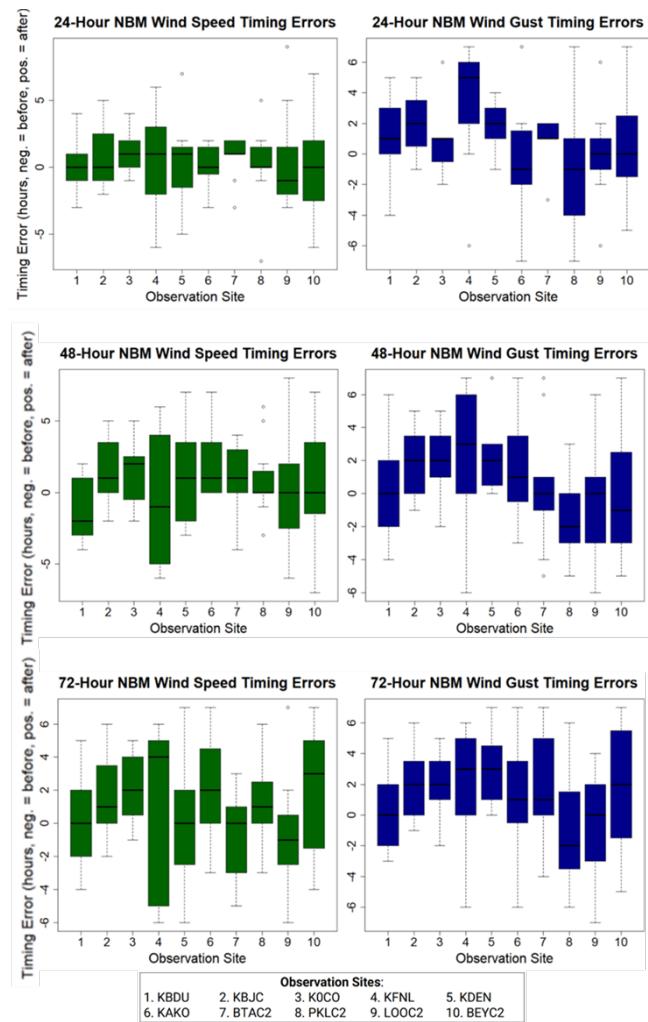

Figure 6. Boxplots of each site's 24 hr, 48 hr, and 72 hr NBM windstorm timing errors. The median of the timing errors is denoted by the solid black line in the middle of the interquartile range (the green and blue boxes), and the minimum and maximum errors are plotted at the ends of the box plot whiskers (bottom and top, respectively). There are notable timing error differences for each site during the 11 windstorms examined, and these variations increase from a 24 hr to 72 hr NBM forecast lead time.

predicts the timing of maximum wind speeds and gusts during downslope windstorms in this region. This result is also revealed in Fig. 7, where the average timing errors for the three different forecast lead times are nearly 0 to 1.25 h too late in accurately determining the time of peak wind speeds and gusts. The lack of a strong agreement among the sites indicates that the timing errors vary for each individual windstorm and each observational site. Therefore, individual windstorm and observational site timing errors can be calculated
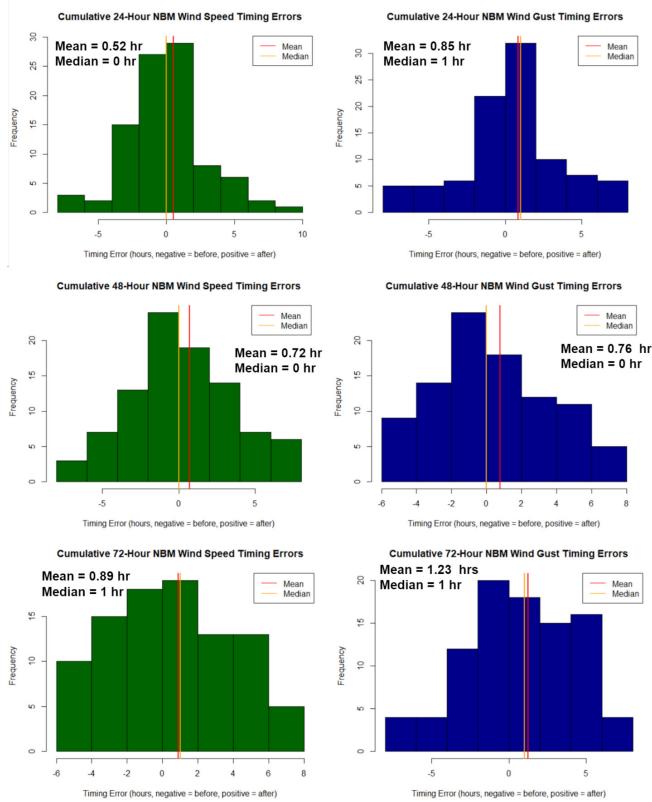
Figure 7. Boxplots of each site's 24 hr, 48 hr, and 72 hr NBM wHistograms of NBM forecasted wind speed (green) and gust (blue) timing errors accumulated across all observational sites, with the mean and median marked by a vertical line in red and yellow, respectively.

and provided to local forecasters for forecast guidance, but there is no systematic bias correction that can be applied uniformly to all sites.

d.   Case study: 22 December 2020

One windstorm that occurred on 22 and 23 December 2020 exhibited strong wind speeds and gusts that reached 41.1 m s^{-1} (92 mph) at the CO109 site, and was poorly forecasted by the NBM to a greater extent than the other windstorms. During this windstorm, an upper-level trough (Fig. 8) as well as a cold front associated with a surface cyclone (Fig. 9) passed over Colorado. Recall that westerly cross-barrier flow with enhanced stability above mountaintop is associated with the development of a chinook, whereas the passage of an upper-level trough and northwesterly flow aloft is associated with the development of a bora. Enhanced wind shear above a stable layer between 600 and 500 mb is evident in the first two Denver International Airport soundings at 1200 UTC 22 December and 0000
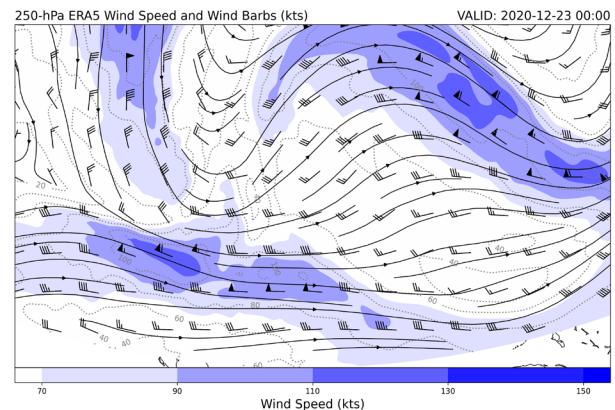

Figure 8. 250 hPa map of ERA5 (Hersbach et al. 2018) geopotential heights and wind speed (shading, barbs) over the continental United States at 0000 UTC on 23 December 2020. Note the upper-level trough moving over the state of Colorado from the west.
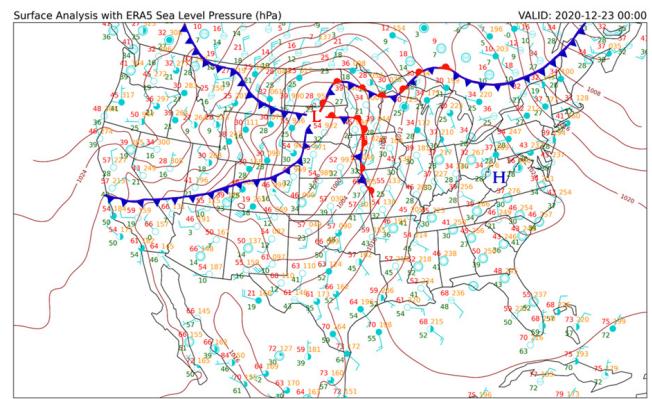

Figure 9. Surface analysis at 0000 UTC on 23 December 2020 across the Continental United States. Note the surface cyclone, and cold front moving from the northwest over Colorado. The location of analyzed fronts is based on the archived Weather Prediction Center (National Weather Service 2023b) analysis at this time.

UTC 23 December 2020 (Fig. 10), and, when combined with increasing cross barrier flow, highlight conditions favorable for a chinook. The 1200 UTC 23 December 2020 sounding features the aforementioned ingredients of a bora. As this trough and cold front moved through the Colorado Front Range, both warm chinook (prefrontal) and cold bora (post-frontal) downslope winds occurred. The HRRR 10 m streamlines from a model run initialized at 0000 UTC 22 December 2020 (24 h prior to the windstorm) show the transition from a chinook to a bora over 5 h in Fig. 11, at least for the lower elevations of Boulder and Jefferson Counties (grey shading in Fig.
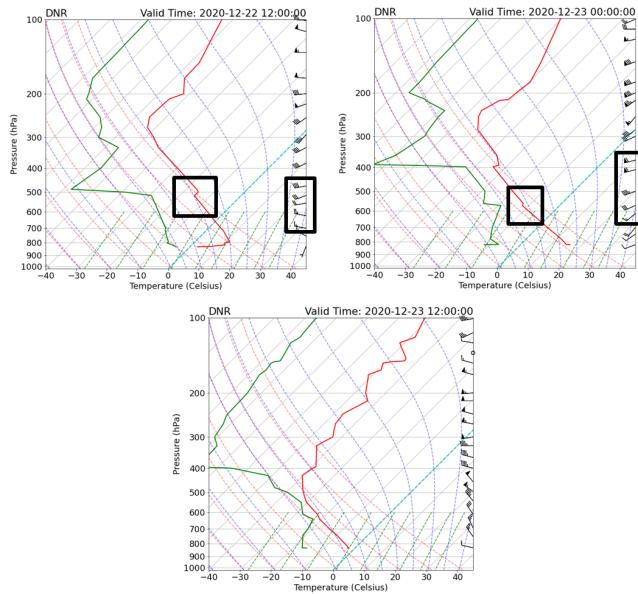
Figure 10. Denver, Colorado soundings from 12 UTC 22 December 2020 to 12 UTC 23 December 2020 at 12 h intervals. The black boxes isolate the inversion layer and the wind shear above 600 hPa supportive of the development of a bora. The lack of these ingredients in the third sounding aligns with the end of the bora across the Colorado Front Range.

11). The peak wind speeds and gusts associated with this windstorm are shown in Tables 1 and 2, respectively, while the observations recorded during this windstorm are shown spatially in Fig. 12. All sites experienced a peak gust of at least 23.2 m s^{-1} (45 kt), with the Buckeye site (BECY2) having the highest peak gust of 33.4 m s^{-1} (65 kt). High wind speeds and gusts were recorded during both the chinook and bora components of the windstorm, but an increase in the wind speeds and gusts across the eastern Colorado Plains, and a coincident decrease in temperature throughout the entire region, are exclusively associated with the bora.

On average for all 10 sites during this windstorm, the NBM was 3.23 h and 2.93 h too late at forecasting the time of the overall peak wind speeds and gusts, respectively. In Fig. 13, the average overall multiplicative bias is below one for all sites and all forecast lead times, implying that the NBM uniformly underestimated the wind speeds and gusts during this windstorm. On average, the wind speeds and gusts during this windstorm were underestimated by approximately one half by the NBM. The average wind speed MAE was 8.0 m s^{-1} (15.5 kt), and the average wind gust MAE was 13.6 m s^{-1} (26.4 kt), with an MAE as high as approximately 21.1 m s^{-1} (41.1 kt) at Buckeye
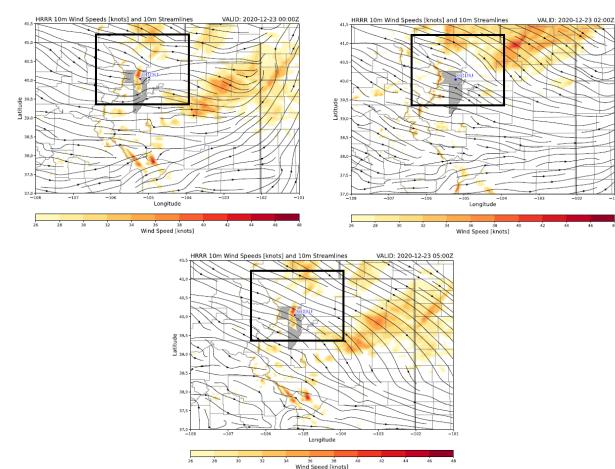

Figure 11. HRRR forecast model runs initialized at 0000 UTC 22 December 2020, showing 10 m streamlines (black lines) and wind speeds (yellow/red shading). Boulder and Jefferson counties are denoted in grey. The selected times of the model run capture the transition of the chinook to a bora. The black box indicates the innermost WRF domain used in this study.

(BEYC2). These are substantial errors that forecasters must recognize and try to mitigate when determining whether watches or warnings should be issued.

e. Case study: WRF simulations

A spatial comparison of the 10 m wind speed for each WRF simulation is shown in Fig. 14 (as well as animations for each simulation in Fig. 15). The model shows agreement among all simulations with respect to the forecasted 10 m wind speed during the first six hours, and all simulations follow a similar evolution throughout the duration of the windstorm (e.g., Fig. 16). The 40 vertical eta levels simulation features a greater overall peak wind speed than the other three simulations during the first six hours as well as an earlier timing of this peak wind speed (i.e., prior to 0000 UTC in the 40-eta level simulation compared to after 0000 UTC in the other simulations). To compare the modeled wind speeds with observational data, Fig. 17 displays a time series of the wind speed at the CO109 observation site as well as at the nearest grid point to the CO109 site within the WRF simulations. In general, the WRF simulations represented the winds at the CO109 site well, with the most notable error being an overestimation of wind speeds at the end of the simulation period (0600 UTC to 1200 UTC on 23 December 2020). Increasing vertical levels in the WRF model from 40 to 73 increased the
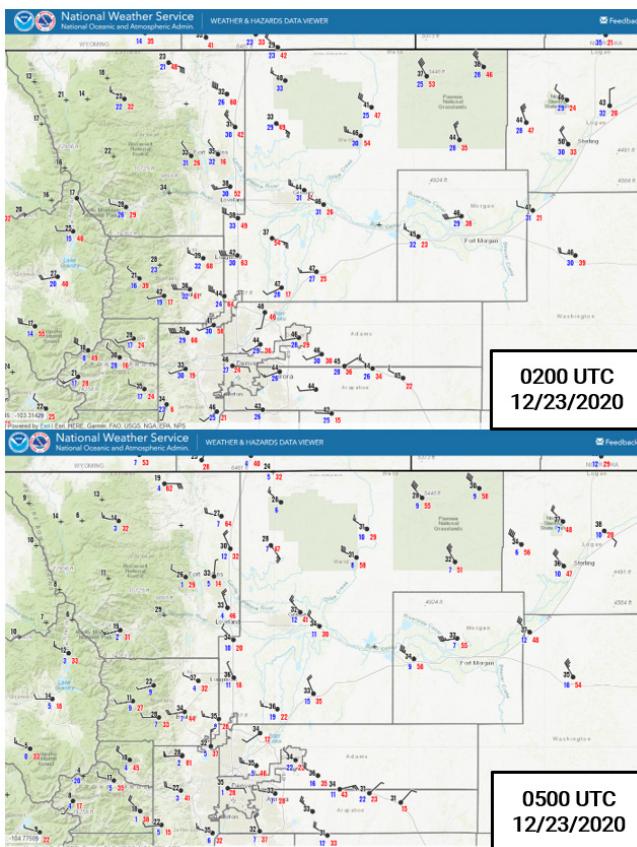
Figure 12. Observations from the downslope windstorm on 22 December 2020. The gusts are shown in red (mph), temperatures (ºF) are shown in black, and dewpoint temperatures (ºF) are shown in blue. The time period shown illustrates the transition from a widespread chinook along the Front Range at 0200 UTC to a bora by 0500 UTC. These observation maps are from the National Weather Service's Weather & Hazards Data Viewer (National Weather Service 2023a).

amount of detail in the spatial distribution of wind speeds associated with the downslope windstorms (Figs. 14 and 15), but changing the user-defined eta levels did not increase the forecasted wind speeds from the model at the CO109 site.

Next, a crucial characteristic of the overall windstorm was the transition from a chinook to a bora, which the WRF simulations capture with some caveats. Specifically, the WRF wind speed for the CO109 site prior to 0000 UTC on 23 December 2020 during the chinook is overestimated by the WRF simulations, whereas the wind speeds during the bora (approximately 0200 UTC to 0600 UTC on 23 December 2020) were underestimated by WRF (Fig. 17). The transition from a chinook to a bora was also well captured by real-time HRRR forecasts (Fig. 11), with the observational data
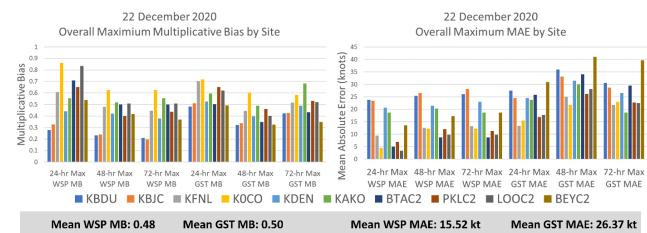

Figure 13. 24 hr, 48 hr, and 72 hr overall maximum multiplicative biases and MAEs for each site during the 22 December 2020 windstorm.
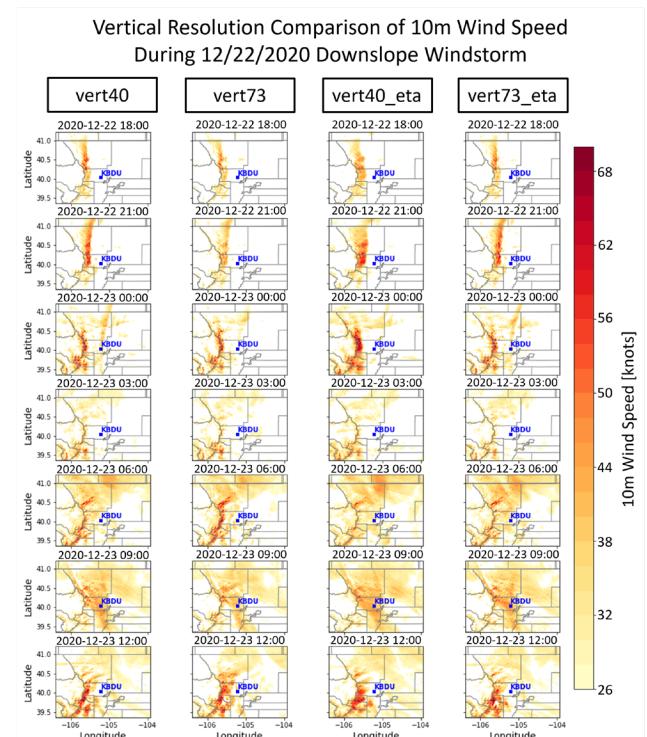

Figure 14. Spatial comparison of the 10-m wind speed for the four WRF simulations (from left to right: 40 vertical levels, 73 vertical levels, 40 eta levels, and 73 eta levels). The chinook windstorm is characterized by the localized stronger winds immediately along the Colorado Front Range. After 0000 UTC 23 December 2020, the stronger wind speeds become more widespread following the passage of an upper-level trough, transitioning the chinook into a bora.

during the windstorm (Fig. 12) showing the arrival of much colder temperatures across the Front Range and much more widespread strong winds after 0000 UTC as a result of the post-frontal bora. Overall, based on a spatial comparison of the WRF simulations (Fig. 14), HRRR forecasts (Fig. 11), and the time series of winds near the CO109 observation site (Fig. 17), it is
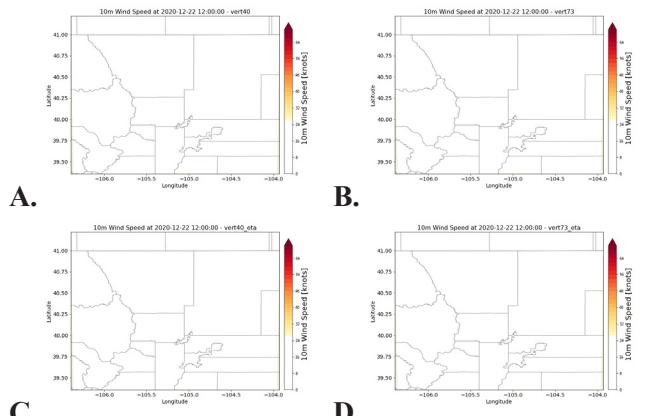
Figure 15. Animations of the four different WRF simulations during the 22 December 2020 downslope windstorm. *Click images for animation*.
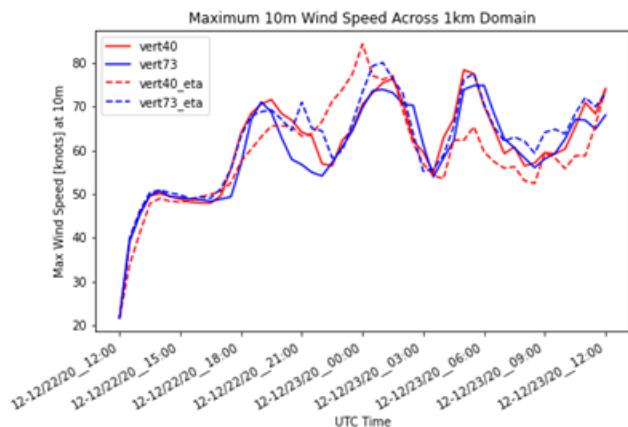

Figure 16. The maximum 10 m wind speed across the 1 km innermost domain as a function of time for each WRF simulation.

Figure 17. The WRF simulations and observed 10 m wind speed at the CO109 observation site during the 22 December 2020 downslope windstorm. The WRF data have 30 min temporal resolution whereas the observational data have 10 min temporal resolution. The CO109 NBM forecast was not available at the time of this study from the NBM 1D Viewer; therefore, the CO109 NBM forecast was not included in this figure. The CO109 (Colorado Department of Transportation observation station) anemometer height was assumed to be 10 m.

shown that forecast models successfully reproduced the transition of a chinook into a bora on 22 December 2020. It is expected that forecast models can reproduce this windstorm transition with fidelity because it is associated with a synoptic-scale frontal passage that should be well resolved by the models. The finer meso- to microscale details of the model run, such as the magnitude of the wind speeds, represent a challenge, however. Even though the timing of the windstorm within the WRF simulations was more accurate than the NBM, the magnitude of the wind speeds produced by the WRF model were either too high or too low when compared against observations.

Furthermore, when compiling the observational data, WRF simulations, and 24 h NBM output for the Broomfield/Jefferson County (KBJC) site during the 22 December 2020 windstorm (Fig. 18), it is shown
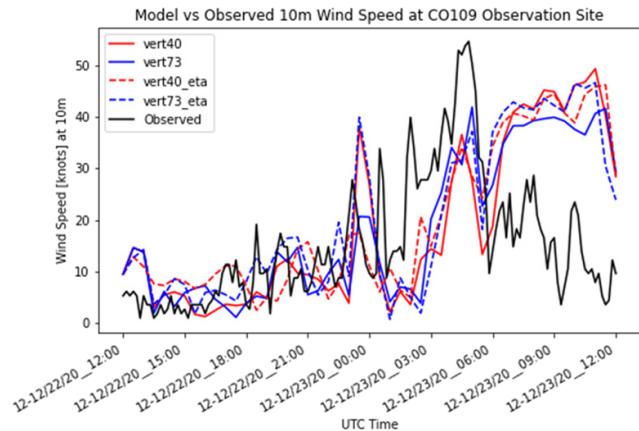
the NBM produced substantially lower wind speeds compared to both the observational data and WRF simulations. The NBM forecast exhibits a slight increase in wind speed throughout the 15 h time period but does not produce individual peaks in the wind speed that match the WRF simulations and observations. Instead, it appears that the chinook and bora components of the windstorm were rather weak within the 24 h NBM forecast. This may be due to the differences in temporal resolution of output between the WRF simulations and the NBM (30 min and one hour for the WRF and NBM, respectively), as well as the coarser horizontal resolution of the NBM (2.5 km). Also, KBJC is approximately 13 km from the foothills of the Colorado Front Range, so the statistical terrain adjustment scheme described in section 3b would not increase wind speeds as much compared to a site located in the foothills or directly adjacent to the terrain (like CO109). Notably, the WRF simulation almost exactly matches the peak wind speed observed at the KBJC site during the chinook (approximately 0100 UTC 23 December 2020) but neglects other peaks in the observed wind speed before and after the chinook. Similar to the CO109 site, the KBJC site also experiences strong winds in the WRF
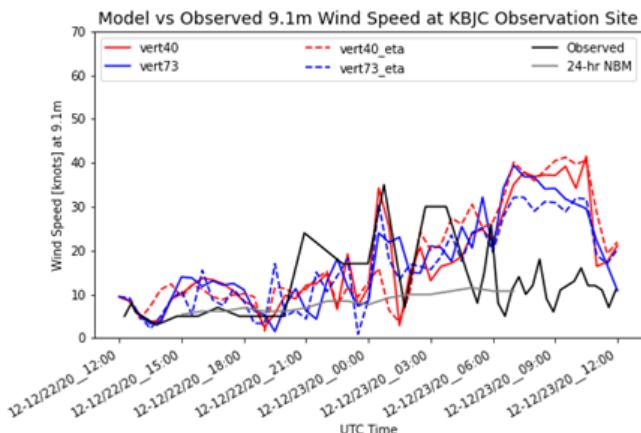
Figure 18. The WRF adjusted 9.1 m wind speed forecasts, observed 9.1 m wind speed, and 24 h NBM adjusted 9.1 m wind speed forecast at the Broomfield/ Jefferson County (KBJC) observation site during the 22 December 2020 downslope windstorm. The WRF data have 30 min temporal resolution, the observational measurements for this site range from one to three times per hour, and the NBM data have one hour temporal resolution.

simulations after 0600 UTC 23 December 2020 that are not actually observed.

4.   Discussion

In this study, eleven downslope windstorms from October 2020 through May 2021 were identified using ten observation sites along the Colorado Front Range. An evaluation of the NBM v4.0 was completed using three methods: a verification of lead hour, hourly maximum, and overall maximum wind speeds and gusts. Correlation tests, MAEs, MBs, and timing errors were calculated for each method and downslope windstorm. From there, four WRF simulations were completed with varied vertical resolutions for a downslope windstorm on 22 December 2020. These simulations were completed because the NBM featured considerable errors forecasting the timing of this windstorm, as well as the magnitude of the observed wind speeds and gusts. Overall, the goal of this exploratory study is to improve downslope windstorm forecasts for the Colorado Front Range through an informed understanding NBM biases and shortcomings during these windstorms from the 2020/2021 cool season.

The NBM performs the most poorly (lowest MB) for the Boulder Municipal Airport (KBDU) and Broomfield/Jefferson County (KBJC) sites (shown in

red in Table 4). The NBM potentially performed the most poorly at these sites because of their close proximity to the mountains, where it may be difficult for the NBM to account for the rapid change in local topography that characterizes these locations due to its 2.5 km horizontal resolution and the need to downscale data from some input models to the NBM. This performance may also imply that smaller scale processes that are parameterized by coarser component models within the NBM could introduce errors due to the assumptions that constitute these parameterizations. The complex multi-scale interactions that characterize downslope windstorms, as well as their quick and high-impact nature, may also cause the NBM to perform poorly at these sites. On the other hand, the NBM performed exceptionally well at Sugarloaf (BTAC2), Pickle Gulch (PKLC2), and Lookout Mountain (LOOC2) (shown in dark blue in Table 4). This may be due to statistical wind adjustments that are applied to the NBM at these mountainous sites, and/or because there was approximately only one observation per hour at each of these sites. The lack of measurements introduces a potential limitation of this analysis, where a singular observation at a site can be used as the lead hour, hourly maximum, and overall maximum observation. Therefore, the NBM may be underestimating or overestimating the wind speeds and gusts at these locations, but a finer temporal resolution at these sites is needed to observe sub-hourly wind variations. Another alternative is to obtain downslope wind data from a longer period of time (i.e., more than one downslope wind season).

From this study, it is apparent that WRF simulations can reproduce chinook and bora winds, which is important because multiple versions of the WRF are included in the NBM. Spatially, increasing the number of vertical levels in the WRF model increased the amount of detail in the spatial distribution of wind speeds along the Colorado Front Range during downslope windstorms, but it did not improve the forecasted 10 m wind speeds at the CO109 observation site compared to observational data. Also, it appears the resultant wind speeds within the WRF model are not sensitive to the method through which eta levels are defined within the model. Given this lack of sensitivity, future work could involve creating WRF ensembles of varying boundary layer schemes or other WRF parameterizations to investigate how the wind speeds during the windstorms change as a function of these parameterizations and the flavor of windstorm (e.g., bora or chinook). Future extensions of this research could also examine how

Table 4. Summary statistics for the overall maximum wind speed (WSP) and gust (GST) average multiplicative biases for each observation site. The sites at which the NBM performed the worst during the 2020-2021 downslope wind season are shown in red (KBDU and KBJC), whereas the best sites are shown in blue (BTAC2, PKLC2, and LOOC2).

Station	KBDU	KBJC	KFNL	K0CO	KDEN	KAKO	BTAC2	PKLC2	LOOC2	BEYC2
WSP Average Overall MB	0.33	0.32	0.54	0.54	0.53	0.64	1.00	0.87	0.86	0.58
GST Average Overall MB	0.48	0.46	0.71	0.62	0.59	0.71	0.84	0.79	0.73	0.59

other observations (besides those at KBJC and CO109) at sites closest to and within the mountains compare with the WRF simulations during the 22 December 2020 windstorm, because the NBM performed the worst or best at these observation sites, respectively.

Our study primarily focuses on a verification of the NBM and an analysis of a single windstorm using WRF, but it is not the only one to use NWP to examine downslope windstorms. Previous downslope wind NWP studies examined the Wasatch winds in Utah (Lawson and Horel 2015), downslope winds leeward of the Medicine Bow Mountains in Wyoming (Pokharel et al. 2017), and Sundowner winds in California (Duine et al. 2019). Lawson and Horel (2015) noted that the inclusion of flow-terrain interactions often improves the predictability of downslope windstorms. Additionally, the presence of large-scale atmospheric phenomena, such as horizontal wave breaking, may help or hinder in forecasting mesoscale processes like downslope windstorms, which is in agreement with earlier studies (Palmer 1993; Doyle et al. 2013; Durran and Gingrich 2014). For instance, forecasters in Utah had an approximately 90 h lead time before the 1 December 2011 Wasatch Downslope Windstorm due to the presence of ideal synoptic-scale conditions that were similar to previous Wasatch windstorms (descending air in lee of the mountains and the lack of a cold layer of air on the leeward side of the mountain) and high confidence in model forecasts. This is in stark contrast to another study in California that estimated lead times to be only approximately 12 h before a downslope windstorm in their case-study region (Reinecke and Durran 2009). Our study examined three forecast lead times (24 h, 48 h, and 72 h) and determined that there is an improvement in the prediction of the magnitude and timing of wind speeds and gusts during downslope windstorms at shorter lead times, but that individual windstorms can still suffer from poor predictability at short lead times with respect to the magnitude of observed wind speeds and gusts.

In terms of the synoptic-scale environment, Pokharel et al. (2017) found that, although upstream large-scale conditions are often indicative of downslope windstorm formation, a self-induced critical level allowed a downslope windstorm on 11 January 2013 in the Medicine Bow Mountains to persist after analyzing observations. They found this result to be true for 19 other downslope windstorm cases in the region, reaching the conclusion that upstream large-scale flow characteristics and stability are not the only factors necessary for the development, persistence, and prediction of a downslope windstorm. For our 22 December 2020 case study, a mid- and upper-level trough passed over northeastern Colorado and strong stability was present near mountaintop, allowing for favorable synoptic-scale conditions for a downslope windstorm along the Colorado Front Range. Yet, despite these favorable synoptic-scale conditions, the WRF simulations did not perfectly align with observations. Finally, Duine et al. (2019) found that using various planetary boundary layer schemes produced similar timing and durations for sundowner winds. However, higher values of roughness length caused by nearby vegetation from land surface models, coupled with boundary layer schemes that account for the interaction between the sundowner winds and the marine boundary layer, provided the most realistic WRF forecast simulations. Consequently, experimenting with the roughness length used within the WRF simulations for this study, as well as utilizing different boundary layer schemes, may produce results that match closer to the observational data.

For the Colorado Front Range, specifically, previous studies have compared model representations of the 11 January 1972 downslope windstorm (Doyle et al. 2000), performed statistical modeling of Boulder downslope winds (Mercer et al. 2008), and examined WRF simulations of the 2013 Boulder Flood (Schwartz 2014). These studies (and those mentioned in the previous paragraph) used at least two nested domains

and similar WRF setups that were the basis for the simulations in this study. Doyle et al. (2000) simulated the dynamics of wave breaking events during the 11 January 1972 Boulder windstorm using 11 non-hydrostatic models and found that their simulations were sensitive to the choice of lateral boundary conditions as well as the numerical dissipation and horizontal advection schemes within the models. In agreement with our results, the authors also found their simulations to be sensitive to vertical resolution, suggesting that finer vertical resolution may be needed to resolve these downslope winds—specifically upper-level gravity wave propagation and breaking—in numerical weather prediction models. Doyle et al. (2000) also noted that slight changes to the shear and stability above 10 km substantially affected the structure of wave-breaking during the 1972 downslope windstorm, further highlighting the importance of vertical resolution for resolving these windstorms. Mercer et al. (2008) used a support vector regression (SVR) model to statistically model downslope windstorms in Boulder and found that their models had root mean square errors (RMSE) <6 m s^{-1} for wind speeds and 12 m s^{-1} for wind gusts 85% of the time. This is consistent with our NBM study, as the NBM had larger MAEs for forecasted wind gusts in comparison to wind speeds. As demonstrated by the previous studies above, downslope windstorms are complex atmospheric phenomena that require additional research to improve understanding and forecasts.

Overall, these findings corroborate Boulder NWS WFO forecasters' experience with the NBM v4.0 during downslope windstorms: the NBM often underestimates winds during these windstorms and does not forecast the timing of the strongest winds accurately, especially at longer lead times. Although the overall statistics compiled from 11 downslope windstorms during the 2020/2021 cool season support these claims, an in-depth case study of the 22 December 2020 windstorm further revealed the poor accuracy of NBM forecasts of downslope windstorms. Furthermore, the inaccurate timing of NBM downslope windstorm forecasts can be noted by forecasters as an NBM bias, and the quantified timing errors in this study may be used to adjust downslope windstorm forecasts accordingly. An updated version of the NBM (v4.1) was recently implemented as of 17 January 2023. This exploratory study can subsequently be used as a baseline during future downslope windstorm seasons to determine if the newer NBM version captures the characteristics of downslope windstorms along the Colorado Front Range

better than the previous version used in this study (v4.0). To preliminarily determine how well the NBM v4.1 performs during Colorado Front Range downslope windstorms compared with v4.0, two NBM v4.1 downslope windstorm verifications were performed. Figure 19 shows the overall maximum MBs for seven of the observational sites that were impacted by a windstorm on 9 March 2023. NBM v4.1 performs well for KBDU, KBJC, KFNL, K0CO, and BEYC2, but it is substantially overestimating wind speeds and gusts, especially at shorter lead times. Furthermore, Fig. 20 shows another MB verification for both v4.1 and v4.0 during a windstorm on 10 January 2023. Since the NBM v4.1 was not widely implemented yet, both versions of the NBM were available to compare their respective performances. Consistent with our study, the NBM v4.0 is often underestimating wind speeds at the majority of the sites, except for BTAC2 and PKLC2. The NBM v4.1 exhibits reduced errors, however, as shown by many of the MBs moving closer to 1. Similar to the 9 March 2023 windstorm (Fig. 19), the BTAC2 and PKLC2 wind speed and gust MBs are higher than the other sites, indicating that v4.1 is overestimating these wind speeds and gusts more than in v4.0. Although this could be due to the limited observational data at these sites (one observation per hour), this overestimation of wind speeds and gusts by the NBM appears in both v4.0 and 4.1, so it would be beneficial to further investigate what is causing the NBM to produce high winds at these mountainous locations. Additionally, an extensive study of one windstorm using the NBM v4.1—similar to the 22 December 2020 windstorm verification shown in this study—could allow us to better understand the strengths and weaknesses of the NBM v4.1 with respect to Colorado Front Range downslope windstorms.
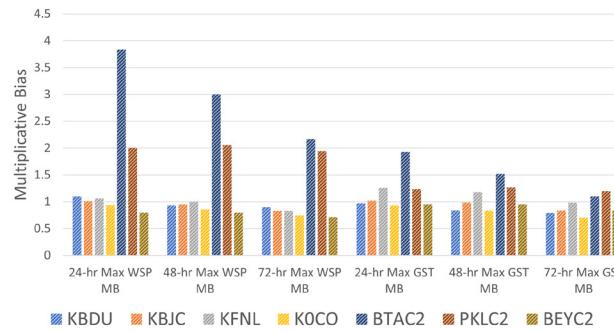

Figure 19. 24 hr, 48 hr, and 72 hr NBM v4.1 overall maximum multiplicative biases for seven sites during the 9 March 2023 windstorm.
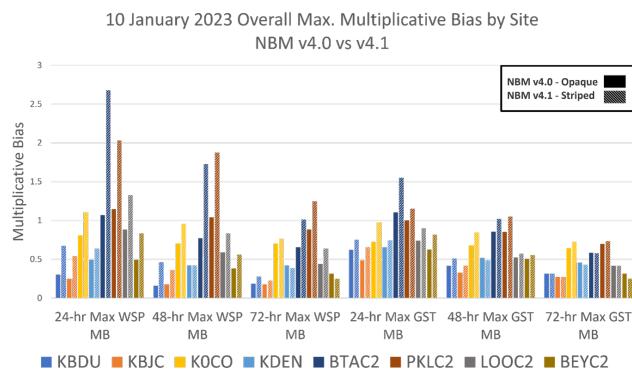
Figure 20. 24 hr, 48 hr, and 72 hr NBM v4.0 (opaque) and v4.1 (striped) overall maximum multiplicative biases for eight sites during the 10 January 2023 windstorm.

This study represents the first NBM forecast verification of downslope winds along the Colorado Front Range and can be applied to other regions, such as the Wasatch Mountains and Santa Ana wind-prone areas, to examine how the NBM performs during other types of downslope windstorms. From this study, it is shown that localized, complex events, such as downslope windstorms, present a challenge for modeling systems that incorporate the blending of multiple weather models. To improve the forecasting of downslope windstorms by the NBM, a larger number of observational sites and better temporal resolution of observations during downslope windstorms along the Colorado Front Range could enable researchers to calibrate the NBM and/or other weather models based on this data. These observations would also improve understanding of the mesoscale variability of downslope windstorm dynamics because there are still many unanswered questions about processes that occur on the sub-grid scale. The removal of global model forecasts from short-term NBM forecasts could also potentially improve the NBM's performance during downslope windstorms because global models feature coarser resolution relative to the higher resolution models blended into the NBM. Another potential method for improving the NBM during downslope windstorms could be to run the higher resolution models out to longer lead times. Two drawbacks to these suggestions are that (1) this can be computationally laborious and expensive, and (2) high resolution models are not always more accurate than global models. Furthermore, verification of not only the NBM, but also other weather models, would help inform forecasters by providing them with how each model is biased during downslope windstorms. Finally, given

the threats posed by anthropogenic climate change, an examination of downslope windstorm environments within climate models, such as the Community Earth System Model (CESM) (Hurrell and Coauthors 2013; Danabasoglu and Coauthors 2020), could assist in the improvement of the climate models' ability to provide a robust representation of these windstorms. These climate model simulations could subsequently be used to investigate how these windstorms would intensify, weaken, or remain the same in a future climate.

5. Conclusions

A study of downslope windstorms along the Colorado Front Range from October 2020 to May 2021 was conducted. This study included statistical verification of NBM forecasts as well as a series of WRF simulations performed for a downslope windstorm on 22 December 2020. Listed below is a summary of the primary implications of this study:

- Forecasts for localized, complex events, such as downslope windstorms, present a challenge for modeling systems that incorporate the blending of multiple weather models.

- For the 2020/2021 cool season, the NBM underestimated wind speeds and gusts for sites located farther east of the Colorado Front Range but performed well for sites embedded within mountainous terrain. The NBM windstorm timing errors varied among observational sites, but the timing errors generally reduced with shorter forecast lead times.

- Verification of not only the NBM, but also other numerical weather prediction models, would help inform forecasters by providing them with a systematic assessment of the degree to which the results of the present study are consistent across other modeling platforms.

Disclaimer. This report was prepared as an account of work sponsored by an agency of the United States Government. Neither the United States Government nor any agency thereof, nor any of their employees, makes any warranty, express or implied, or assumes any legal liability or responsibility for the accuracy, completeness, or usefulness of any information, apparatus, product, or process disclosed, or represents that its use would not infringe privately owned rights. Reference herein to any specific commercial product, process, or service by trade name, trademark, manufacturer, or otherwise does not necessarily constitute or imply its endorsement, recommendation, or favoring by the United States Government or any agency thereof. The views and opinions of authors expressed herein do not necessarily state or reflect those of the United States Government or any agency thereof.

––––––––––––––––––

REFERENCES

Brinkmann, W. A. R., 1971: What Is a foehn? *Weather*, **26**, 230–240, CrossRef.

––––, 1974: Strong downslope winds at Boulder, Colorado. *Mon. Weather Rev*., **102**, 592–602, CrossRef.

Brower, M., 2012: Wind resource assessment: a practical guide to developing a wind project. Wiley, Hoboken, 280 pp. CrossRef.

Cao, Y., and R. G. Fovell, 2016: Downslope windstorms of San Diego County. Part I: a case study. Monthly Weather Review, 144, 529–552, CrossRef.

––––, and ––––, 2018: Downslope windstorms of San Diego County. Part II: physics ensemble analyses and gust forecasting. *Weather and Forecasting*, **33**, 539–559, CrossRef.

Craven, J. P., D. E. Rudack, and P. E. Shafer, 2020: National Blend of Models: a statistically post-processed multi-model ensemble. *J. Oper. Meteor*., 1–14, CrossRef.

Danabasoglu, G., and Coauthors, 2020: The Community Earth System Model Version 2 (CESM2). *Journal of Advances in Modeling Earth Systems*, **12**, 2019MS001916, CrossRef.

Doyle, J. D., and Coauthors, 2000: An intercomparison of model-predicted wave breaking for the 11 January 1972 Boulder Windstorm. *Mon. Weather Rev*., **128**, 901–914, CrossRef.

––––, C. C. Epifanio, A. Persson, P. A. Reinecke, & G. Zängl, 2013: Mesoscale modeling over complex terrain: numerical and predictability perspectives. *Mountain Weather Research and Forecasting: Recent Progress and Current Challenges*, F.K. Chow, S.F.J. De Wekker, and B.J. Snyder, Eds., Springer Atmospheric Sciences, Springer Netherlands, 531–589. CrossRef.

Duine, G.-J., C. Jones, L. M. Carvalho, and R. G. Fovell, 2019: Simulating sundowner winds in coastal Santa Barbara: model validation and sensitivity. *Atmosphere*, **10**, CrossRef.

Durran, D. R., 1990: Mountain waves and downslope winds. Atmospheric Processes over Complex Terrain, R.M. Banta et al., Eds., *Meteorological Monographs*, **23**, American Meteorological Society, 59–81. CrossRef.

––––, and M. Gingrich, 2014: Atmospheric predictability: why butterflies are not of practical importance. *J. Atmospheric Sci*., **71**, 2476–2488, CrossRef.

Fovell, R. G., M. J. Brewer, and R. J. Garmong, 2022: The December 2021 Marshall Fire: predictability and gust forecasts from operational models. *Atmosphere*, **13**, 765, CrossRef.

Glossary of Meteorology, 2012: Downslope wind. *Gloss. Meteorol*.,. [Available online at: glossary.ametsoc.org/wiki/Downslope_wind]. (Accessed 3 November 2021).

Goger, B., M. W. Rotach, A. Gohm, I. Stiperski, and O. Fuhrer, 2016: Current challenges for numerical weather prediction in complex terrain: topography representation and parameterizations. *2016 International Conference on High Performance Computing Simulation (HPCS)*, 2016 International Conference on High Performance Computing Simulation (HPCS), Innsbruck, Austria, 890–894. CrossRef.

Hersbach, H., B. Bell, and Coauthors, 2018: ERA5 hourly data on pressure levels from 1959 to present. Copernicus Climate Change Service (C3S) Climate Data Store (CDS). (Accessed on 20 January 2023), CrossRef.

Horel, J., and Coauthors, 2002a: MESOWEST: cooperative mesonets in the western United States. *Bull. Amer. Meteor. Soc*., **83**, 211–226, CrossRef.

––––, T. Potter, L. Dunn, W. J. Steenburgh, M. Eubank, M. Splitt, and J. Onton, 2002b: Weather support for the 2002 Winter Olympic and Paralympic Games. *Bull. Amer. Meteor. Soc*., **83**, 227–240, CrossRef.

Hurrell, J. W., and Coauthors, 2013: The Community Earth System Model: a framework for collaborative research. *Bull. Amer. Meteor. Soc.*, **94**, 1339–1360, CrossRef.

Iacono, M. J., J. S. Delamere, E. J. Mlawer, M. W. Shephard, S. A. Clough, and W. D. Collins, 2008: Radiative forcing by long-lived greenhouse gases: Calculations with the AER radiative transfer models. *J. Geophys. Res. Atmospheres*, **113**, CrossRef.

Ives, R. L., 1950: Frequency and physical effects of Chinook winds in the Colorado High Plains Region. *Ann. Assoc. Am. Geogr.*, **40**, 293–327, CrossRef.

Janjić, Z. I., 1994: The Step-Mountain Eta Coordinate Model: further developments of the convection, viscous sublayer, and turbulence closure schemes. *Mon. Weather Rev.*, **122**, 927–945, CrossRef.

——, 1996: The surface layer in the NCEP Eta Model. *11th Conference on Numerical Weather Prediction*, 19–23 August 1996. Norfolk, VA: Amer. Meteor. Soc., pp 354–355.

——, 2001: Nonsingular implementation of the Mellor-Yamada level 2.5 scheme in the NCEP Meso model. NCEP Office Note #437, 61 pp. [Available online at: repository.library.noaa.gov/view/noaa/11409].

Kain, J. S., 2004: The Kain–Fritsch convective parameterization: an update. *J. Appl. Meteor. Climatol.*, **43**, 170–181, CrossRef.

Ladwig, W., 2017: wrf-python (Version 1.3.2). : UCAR/NCAR, Boulder, Colorado. CrossRef.

Lawson, J., and J. Horel, 2015: Analysis of the 1 December 2011 Wasatch Downslope Windstorm. *Wea. Forecasting*, **30**, 115–135, CrossRef.

Lundquist, J. K., 2022: Wind shear and wind veer effects on wind turbines. *Handbook of Wind Energy Aerodynamics*, B. Stoevesandt, G. Schepers, P. Fuglsang, and Y. Sun, Eds., Springer International Publishing, 859–880. CrossRef.

Mercer, A. E., M. B. Richman, H. B. Bluestein, and J. M. Brown, 2008: Statistical modeling of downslope windstorms in Boulder, Colorado. *Wea. Forecasting*, **23**, 1176–1194, CrossRef.

Monin, A. S. and A. M. Obukhov, 1954: Basic laws of turbulent mixing in the surface layer of the atmosphere. Contribution of Geophysical Institute of the Academy of Sciences of the USSR, **151**, 163–187. (English translation available online at: https://gibbs.science/efd/handouts/monin_obukhov_1954.pdf]

Muñoz-Esparza, D., R. D. Sharman, and J. K. Lundquist, 2018: Turbulence dissipation rate in the atmospheric boundary layer: observations and WRF mesoscale modeling during the XPIA Field Campaign. *Mon. Wea. Rev.*, **146**, 351–371, CrossRef.

National Centers for Environmental Information, 2020: Global Forecast System (GFS). National Centers for Environmental Information (NCEI). (Accessed 3 February 2023). Available online at: www.ncei.noaa.gov/products/weather-climate-models/global-forecast]

National Oceanic and Atmospheric Administration, 2021: NBM 1D Viewer. (Accessed January 18, 2023). [Available online at: hwp-viz.gsd.esrl.noaa.gov/wave1d/].

——, 2022: Boulder Wind Events: NOAA Physical Sciences Laboratory. (Accessed 23 March 23 2023). [Available online at: psl.noaa.gov/boulder/wind.html].

National Weather Service, 2022: Denver/Boulder, CO climate NOWData. (Accessed 30 September 2022). [Available online at: www.weather.gov/wrh/climate?wfo=bou].

——, 2023a: NWS Weather & Hazards. (Accessed 20 January 2023). [Available online at: www.wrh.noaa.gov/map/].

——, 2023b: WPC Surface Analysis Archive. (Accessed February 21, 2023). [Available online at: www.wpc.ncep.noaa.gov/archives/web_pages/sfc/sfc_archive_maps].

NCEP Central Operations, 2023: NCEP Data Products NAM. (Accessed 3 February 2023). [Available online at: www.nco.ncep.noaa.gov/pmb/products/nam/].

NOAA Meteorological Development Laboratory, 2021: National Blend of Models MDL Virtual Lab. (Accessed December 22, 2021). [Available online at: vlab.noaa.gov/web/mdl/nbm].

——, NBM v4.1 Weather Elements MDL Virtual Lab. (Accessed 9 August 2023). [Available online at: vlab.noaa.gov/web/mdl/nbm-weather-elements-v4.1].

Palmer, T. N., 1993: Extended-range atmospheric prediction and the Lorenz Model. *Bull. Amer. Meteor. Soc.*, **74**, 49–66. CrossRef.

Pokharel, B., B. Geerts, X. Chu, and P. Bergmaier, 2017: Profiling radar observations and numerical simulations of a downslope wind storm and rotor on the lee of the Medicine Bow Mountains in Wyoming. *Atmosphere*, **8**, 39, CrossRef.

Reinecke, P. A., and D. R. Durran, 2009: Initial-condition sensitivities and the predictability of downslope winds. *J. Atmos. Sci.*, **66**, 3401–3418, CrossRef.

Schwartz, C. S., 2014: Reproducing the September 2013 record-breaking rainfall over the Colorado Front Range with high-resolution WRF forecasts. *Weather Forecast.*, **29**, 393–402, CrossRef..

Skamarock, W., and Coauthors, 2008: *A Description of the Advanced Research WRF Version 3*. UCAR/NCAR. CrossRef.

Stull, R., 2017: *Practical Meteorology: An Algebra-based Survey of Atmospheric Science*. 1.02b. Univ. of British Columbia, 940 pp. [Available online at: https://www.eoas.ubc.ca/books/Practical_Meteorology/].

Tewari, M., and Coauthors, 2004: Implementation and verification of the unified Noah land surface model in the WRF model. *20th Conference on Weather Analysis and Forecasting/16th Conference on Numerical Weather Prediction*, Boston, MA: American Meteorological Society. [Available online at: ams.confex.com/ams/84Annual/techprogram/paper_69061.htm].

Thompson, G., P. R. Field, R. M. Rasmussen, and W. D. Hall, 2008: Explicit forecasts of winter precipitation using an improved bulk microphysics scheme. Part II: implementation of a new snow parameterization. *Mon. Wea. Rev.*, **136**, 5095–5115, CrossRef.

UCAR/COMET, 2016: Statistical Methods in the NWS National Blend of Global Models. (Accessed 4 April 2023). [Available online at: https://www.meted.ucar.edu/nwp/blend_statistics/navmenu.php?tab=1&page=5-1-2&type=flash].

——, 2019: NBM v3.2 Modified blend methods and new model components. (Accessed 4 April 2023). [Available online at: www.meted.ucar.edu/nwp/blend_v32_methods/print.php#page_2-1-0].

United States Department of Commerce, 2022: High winds and Marshall Fire on December 30th, 2021. (Accessed 9 March 2022). [Available online at: www.weather.gov/bou/HighWinds12_30_2021].

——, 2023: Greater than the Sum of its Parts... The NWS National Blend of Models. (Accessed 18 January 2023). [Available online at: www.weather.gov/news/200318-nbm32].

Whiteman, C. D., and J. G. Whiteman, 1974: An historical climatology of damaging downslope windstorms at Boulder, Colorado. NOAA Technical Report ERL: 336. National Oceanic and Atmospheric Administration. (Accessed September 1, 2021). [Available online at: repository.library.noaa.gov/view/noaa/18852].